

Bayesian Inference on Group Differences in Brain Networks

Daniele Durante* and David B. Dunson†

Abstract. Network data are increasingly measured along with other variables of interest. Our motivation is drawn from neurophysiology studies measuring a brain activity network for each subject along with a categorical variable, such as presence or absence of a neuropsychiatric disease, creativity groups or type of ability. We develop a Bayesian approach for inferences on group differences in the network structure, allowing global and local hypothesis testing adjusting for multiplicity. Our approach allows the probability mass function for network-valued data to shift nonparametrically between groups, via a dependent mixture of low-rank factorizations. An efficient Gibbs sampler is defined for posterior computation. We provide theoretical results on the flexibility of the model and assess testing performance in simulations. The approach is applied to provide novel results showing relationships between human brain networks and creativity.

Keywords: Brain Network, Mixture model, Multiple testing, Neuroscience, Non-parametric Bayes.

1 Introduction

1.1 Brain networks and creativity groups

Recent advances in brain imaging technologies have played a key role in stimulating current research in neuroscience, while providing evidence against the modular paradigm which considers brain regions as independent actors in specific cognitive functions (Fuster, 2000). This has motivated an increasing consensus within the neuroscience community away from monitoring the level of activity in specific brain regions and towards studying structural brain connectivity networks (connectomes), with cognitive processes a result of interconnected circuits rather than the expression of specialized brain regions (Bressler and Menon, 2010).

Brain connectivity data are now available to facilitate this task, with non-invasive imaging technologies, such as structural magnetic resonance imaging (sMRI), diffusion tensor imaging (DTI) and magnetization-prepared gradient-echo (MP-RAGE) sequence, providing accurate brain network data at increasing spatial resolution; see Stirling and Elliott (2008), Craddock et al. (2013) and Wang et al. (2014) for an overview and recent developments on these brain scanning technologies. Recent studies measure brain networks along with categorical variables, such as the presence or absence of a neuropsychy-

* University of Padua, Department of Statistical Sciences. Via Cesare Battisti, 241, 35121 Padua, Italy. e-mail: durante@stat.unipd.it

† Duke University, Department of Statistical Science. Box 9025, Durham, NC 27708-0251 USA e-mail: dunson@duke.edu

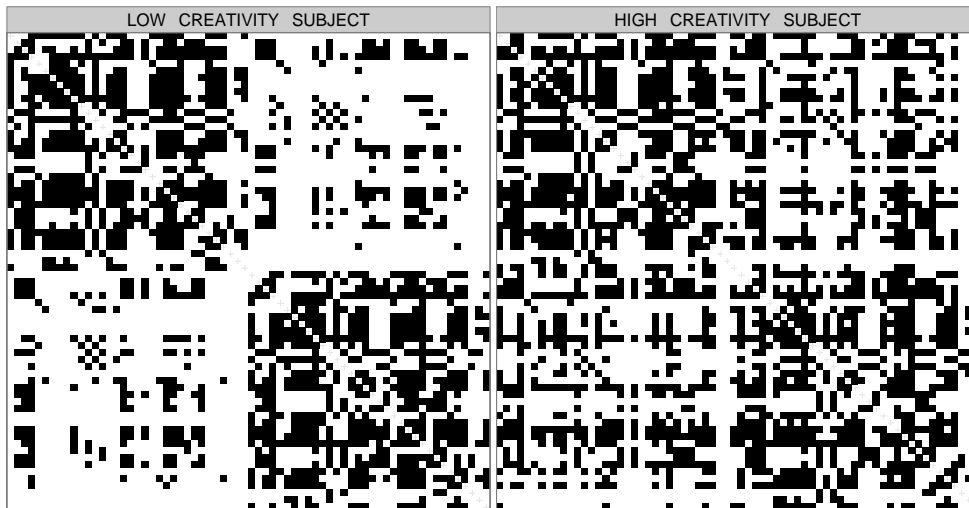


Figure 1: Adjacency matrices A_i representing the brain network for two subjects in different creativity groups. Black refers to an edge and white to a non-edge.

chiatric disease or behavioral state or categorized ability scores, including creativity and different aspects of intelligence. In such studies, there is a need for methods assessing how the brain connectivity structure varies across groups.

We are specifically interested in studying the relationship between the brain connectivity structure and creativity. For subject i ($i = 1, \dots, n$), data consist of the creativity group y_i and an adjacency matrix A_i representing the undirected brain network. We focus on dataset MRN-111 available at <http://openconnecto.me/data/public/MR/>, preselecting subjects having high (> 111 , $y_i = 2$) or low (< 90 , $y_i = 1$) creativity scores. The first group comprises 19 subjects and the second 17, with thresholds chosen to correspond to 15% and 85% quantiles. Creativity scores are measured via the composite creativity index (CCI) (Jung et al., 2010). The brain networks are instead obtained by processing structural MP-RAGE and DTI brain scans via a recently developed pipeline (Roncal et al., 2013) to obtain symmetric adjacency matrices A_i , $i = 1, \dots, n$, with elements $A_{i[vu]} = A_{i[uv]} = 1$ if there is at least one white matter fiber connecting brain regions v ($v = 2, \dots, V$) and u ($u = 1, \dots, v - 1$) in individual i and $A_{i[vu]} = A_{i[uv]} = 0$ otherwise. In our application $V = 68$ and each node in the network characterizes a specific brain region according to the Desikan atlas (Desikan et al., 2006), with the first 34 in the left hemisphere and the remaining 34 in the right; see Figure 1 for an illustration. We are interested in assessing evidence of differences in brain connectivity between the low and high creativity groups, while additionally inferring the types of differences and learning which connections are responsible for these variations.

There has been some emphasis in the literature on developing methods for addressing these goals; see Bullmore and Sporns (2009), Stam (2014) and the references

cited therein for an overview. The main focus is on reducing \mathbf{A}_i to summary statistics $\boldsymbol{\theta}_i = (\theta_{i1}, \dots, \theta_{ip})^T$ ($i = 1, \dots, n$) and then applying exponential random graphs (Simpson et al., 2012) or standard multivariate analyses such as MANOVA (see e.g. Krzanowski, 1988) to test for variations of these statistics across groups. Summary statistics are commonly chosen to represent global network characteristics, such as the number of connections, average path length and clustering coefficient (Rubinov and Sporns, 2010). Similar procedures have been recently employed in exploring the relation between the brain network and neuropsychiatric diseases, such as Parkinson’s (Olde Dubbelink et al., 2014) and Alzheimer’s (Daianu et al., 2013), but analyses are sensitive to the chosen network topological measures, with substantially different results obtained for different types of summary statistics. Moreover, inference is available only on the scale of these topological measures, which typically discards important information about the brain connectivity architecture that may crucially explain differences among groups. For example, Arden et al. (2010) reviews inconsistencies in results relating brain connectivity networks to creative reasoning.

An alternative approach is to avoid discarding information by separately testing for differences between groups in each edge probability while adjusting the significance threshold for multiple testing via false discovery rate (FDR) control (Genovese et al., 2002). As there are $V(V-1)/2$ pairs of brain regions under study, with $V = 68$ using the Desikan atlas (Desikan et al., 2006), the number of tests is substantial. Such massively univariate approaches do not exploit network information, leading to low power (Fornito et al., 2013), and substantially underestimating the variations of the brain architecture across groups. Recent proposals try to gain power by replacing the common Benjamini and Hochberg approach (Benjamini and Hochberg, 1995), with thresholding procedures that account for the network structure in the data (Zalesky et al., 2010). However, such approaches require careful interpretation, while being highly computationally intensive and complex, requiring permutation testing and choice of suprathreshold links.

As there is no gold standard in testing for group differences in brain networks, our contribution aims to overcome previous issues by providing a fully generative Bayesian joint modeling approach for the data (y_i, \mathbf{A}_i) , $i = 1, \dots, n$, which explicitly models the networks instead of reducing data to summary measures prior to statistical analysis, while facilitating inference and testing on changes in the network connectivity structure across groups.

1.2 Statistical modeling of network-valued random variables

A rich variety of models have been considered for a single network, including exponential random graphs (Erdős and Rényi, 1959; Holland and Leinhardt, 1981; Frank and Strauss, 1986), stochastic block models (Nowicki and Snijders, 2001) and latent space models (Hoff et al., 2002). Such approaches have been recently generalized to more complex data structures. Examples include dynamic networks (Robins and Pattison, 2001; Xing et al., 2010; Durante and Dunson, 2014b), where data are available via time-varying adjacency matrices; multiview networks (Tang et al., 2011) in which the dataset is characterized by multiple network views, with each view measuring a differ-

ent type of relationship on the same set of nodes; and population of networks (Durante et al., 2015) when the replicated network data consist of measurements of the same type of network on different individuals. When node- or edge-specific variables are available, these variables can impact the edge probabilities (Snijders et al., 2006; Hoff et al., 2002; Durante and Dunson, 2014a).

In our motivating application, we do not have brain region- or connection-specific information, but instead observe a categorical predictor y_i denoting low or high creativity for the subject. We are interested in defining a fully general nonparametric model for the joint probability mass function (pmf) of the random variable generating data (y_i, \mathbf{A}_i) , $i = 1, \dots, n$. This problem is more closely related to the literature on nonparametric Bayes modeling of multivariate categorical data (Dunson and Xing, 2009). In particular, we can characterize data (y_i, \mathbf{A}_i) , $i = 1, \dots, n$ as unstructured categorical vectors and provide inference on the associated pmf via Dunson and Xing (2009), but this would fail to exploit the network structure and not accommodate efficient testing.

We instead explicitly consider network information in our model formulation, allowing testing on the association between the connectivity architecture and the categorical predictor, while borrowing information across subjects in learning the network structure. This is accomplished by factorizing the joint pmf for the random variable generating data (y_i, \mathbf{A}_i) , $i = 1, \dots, n$ as the product of the marginal pmf of the categorical predictor and the conditional pmf for the network-valued random variable given the group membership defined by the categorical predictor. By modeling the collection of group-dependent pmfs for the network-valued random variable via a flexible mixture of low-rank factorizations with group-specific mixing probabilities, we develop simple testing procedures for global and local variations, while preserving the dependence structure within the network also under the null hypothesis of no variations of the network structure across groups.

In Section 2 we provide the model formulation via dependent mixture of low-rank factorizations and describe the testing procedures. Prior specification, theoretical properties and posterior computation are considered in Section 3. Section 4 provides simulations to assess model performance and testing behavior. Results for our motivating neuroscience application are discussed in Section 5. Concluding remarks are provided in Section 6.

2 Model formulation and testing

2.1 Dependent mixture of low-rank factorizations

Let (y_i, \mathbf{A}_i) represent the group membership and the undirected network observation, respectively, for the i th subject, $i = 1, \dots, n$, with $y_i \in \mathbb{Y} = \{1, \dots, K\}$ and \mathbf{A}_i the $V \times V$ adjacency matrix characterizing the edges in the network. As the brain network structure is available via undirected edges and self-relationships are not of interest, we model (y_i, \mathbf{A}_i) by focusing on the random variable $\{\mathcal{Y}, \mathcal{L}(\mathcal{A})\}$ generating data $\{y_i, \mathcal{L}(\mathbf{A}_i)\}$ with $\mathcal{L}(\mathbf{A}_i) = (A_{i[21]}, A_{i[31]}, \dots, A_{i[V1]}, A_{i[32]}, \dots, A_{i[V2]}, \dots, A_{i[V(V-1)]})^T \in$

$\mathbb{A}_V = \{0, 1\}^{V(V-1)/2}$ the vector encoding the lower triangular elements of \mathbf{A}_i , which uniquely define the network as $A_{i[vu]} = A_{i[uv]}$ for every $v = 2, \dots, V$, $u = 1, \dots, v-1$ and $i = 1, \dots, n$.

Let $\mathbf{p}_{\mathcal{Y}, \mathcal{L}(\mathcal{A})}$ be the joint pmf for the random variable $\{\mathcal{Y}, \mathcal{L}(\mathcal{A})\}$ with $p_{\mathcal{Y}, \mathcal{L}(\mathcal{A})}(y, \mathbf{a}) = \Pr\{\mathcal{Y} = y, \mathcal{L}(\mathcal{A}) = \mathbf{a}\}$, $y \in \mathbb{Y}$ and $\mathbf{a} \in \mathbb{A}_V$ a network configuration. We seek to develop a flexible representation for $\mathbf{p}_{\mathcal{Y}, \mathcal{L}(\mathcal{A})}$, which efficiently exploits network information, favors dimensionality reduction and accommodates simple testing procedures for assessing global and local associations between \mathcal{Y} and $\mathcal{L}(\mathcal{A})$. According to these aims, we factorize $\mathbf{p}_{\mathcal{Y}, \mathcal{L}(\mathcal{A})}$ as

$$p_{\mathcal{Y}, \mathcal{L}(\mathcal{A})}(y, \mathbf{a}) = p_{\mathcal{Y}}(y)p_{\mathcal{L}(\mathcal{A})|y}(\mathbf{a}) = \Pr(\mathcal{Y} = y)\Pr\{\mathcal{L}(\mathcal{A}) = \mathbf{a} \mid \mathcal{Y} = y\}, \quad (2.1)$$

for every $y \in \mathbb{Y}$ and $\mathbf{a} \in \mathbb{A}_V$. It is always possible to characterize the joint pmf $\mathbf{p}_{\mathcal{Y}, \mathcal{L}(\mathcal{A})} \in \mathcal{P}_{K \times |\mathbb{A}_V|}$ as the product of the marginal $\mathbf{p}_{\mathcal{Y}} \in \mathcal{P}_K$ for the grouping variable and the conditional pmfs $\mathbf{p}_{\mathcal{L}(\mathcal{A})|y} \in \mathcal{P}_{|\mathbb{A}_V|}$ of the network-valued random variable given the group membership $y \in \mathbb{Y}$. This also favors inference on how the network structure varies across the K groups, with $\mathbf{p}_{\mathcal{L}(\mathcal{A})|y}$, $y = 1, \dots, K$ fully characterizing such variations. Although we treat \mathcal{Y} as a random variable through a prospective likelihood, the method we propose is valid for inference on differences across groups in network data also for studies that sample groups under a retrospective design.

The marginal probability $\mathbf{p}_{\mathcal{Y}}$ assigned to the K groups is straightforward to represent, and the challenge arises in modeling the collection of pmfs $\mathbf{p}_{\mathcal{L}(\mathcal{A})|y}$, $y = 1, \dots, K$ characterizing the distribution of the network-valued random variable in each group y . For every group $y \in \mathbb{Y}$, one needs a parameter $p_{\mathcal{L}(\mathcal{A})|y}(\mathbf{a})$ for each network configuration $\mathbf{a} \in \mathbb{A}_V$ to uniquely characterize $\mathbf{p}_{\mathcal{L}(\mathcal{A})|y}$, with the number of possible configurations being $|\mathbb{A}_V| = 2^{V(V-1)/2}$. Recalling our motivating applications, $2^{68(68-1)/2} - 1 = 2^{2278} - 1$ parameters are required to uniquely define the pmf of the brain network in each group $y \in \mathbb{Y}$ under the usual restriction $\sum_{\mathbf{a} \in \mathbb{A}_V} p_{\mathcal{L}(\mathcal{A})|y}(\mathbf{a}) = 1$. Clearly this number of parameters is massively larger than the sample size.

To address this dimensionality issue in modeling of the network's pmf without a categorical response, Durante et al. (2015) proposed a mixture of low-rank factorizations. We generalize this approach to characterize changes of $\mathcal{L}(\mathcal{A})$ across groups, while accommodating testing of the null hypothesis of no global association between \mathcal{Y} and $\mathcal{L}(\mathcal{A})$, $H_0 : \mathbf{p}_{\mathcal{Y}, \mathcal{L}(\mathcal{A})} = \mathbf{p}_{\mathcal{Y}}\mathbf{p}_{\mathcal{L}(\mathcal{A})}$ against the alternative of some association $H_1 : \mathbf{p}_{\mathcal{Y}, \mathcal{L}(\mathcal{A})} \neq \mathbf{p}_{\mathcal{Y}}\mathbf{p}_{\mathcal{L}(\mathcal{A})}$, where $\mathbf{p}_{\mathcal{L}(\mathcal{A})}$ denotes the marginal pmf for the network-valued random variable $p_{\mathcal{L}(\mathcal{A})}(\mathbf{a}) = \Pr\{\mathcal{L}(\mathcal{A}) = \mathbf{a}\}$. This is accomplished by letting

$$p_{\mathcal{L}(\mathcal{A})|y}(\mathbf{a}) = \Pr\{\mathcal{L}(\mathcal{A}) = \mathbf{a} \mid \mathcal{Y} = y\} = \sum_{h=1}^H \nu_{hy} \prod_{l=1}^{V(V-1)/2} \left\{ \pi_l^{(h)} \right\}^{a_l} \left\{ 1 - \pi_l^{(h)} \right\}^{1-a_l}, \quad (2.2)$$

for each group $y = 1, \dots, K$ and configuration $\mathbf{a} \in \mathbb{A}_V$, where $(\nu_{1y}, \dots, \nu_{Hy})^T \in \mathcal{P}_H$ is a vector of mixing probabilities specific to group y and $\pi_l^{(h)} \in (0, 1)$ defines the probability of an edge among the l th pair of nodes in the mixture component h , for each $l = 1, \dots, V(V-1)/2$ and $h = 1, \dots, H$.

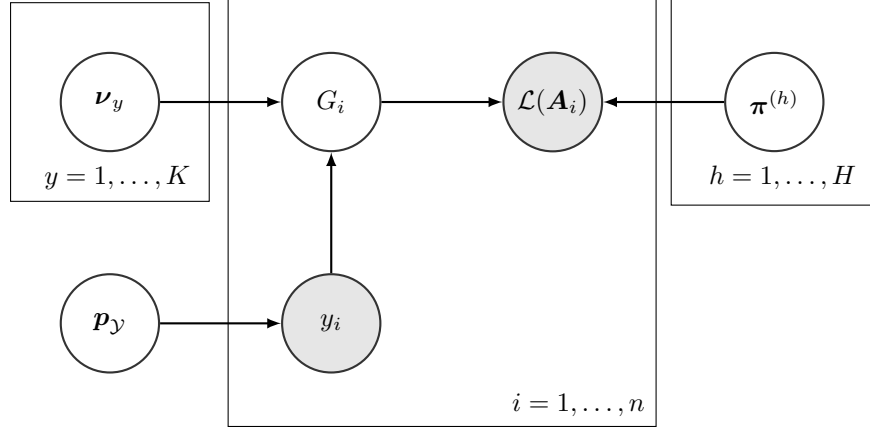


Figure 2: Graphical representation of the probabilistic mechanism generating data $\{y_i, \mathcal{L}(\mathbf{A}_i)\}$, $i = 1, \dots, n$ under factorization (2.1)-(2.2) for the pmf of the random variable $\{\mathcal{Y}, \mathcal{L}(\mathcal{A})\}$.

Figure 2 outlines the mechanism to generate data $\{y_i, \mathcal{L}(\mathbf{A}_i)\}$ from the random variable $\{\mathcal{Y}, \mathcal{L}(\mathcal{A})\}$ with pmf factorized as in (2.1)-(2.2). According to Figure 2 the group indicator y_i is sampled from the categorical random variable with K levels and pmf \mathbf{p}_Y . The network $\mathcal{L}(\mathbf{A}_i)$ is instead generated conditioned on y_i under the mixture representation in (2.2). In particular, given $y_i = y$ we first choose a mixture component by sampling the latent class indicator $G_i \in \{1, \dots, H\}$ from $p_{G|y}$ with $p_{G|y}(h) = \text{pr}(G = h | \mathcal{Y} = y) = \nu_{hy}$. Then, given $G_i = h$ and the corresponding edge probability vector $\boldsymbol{\pi}^{(h)} \in (0, 1)^{V(V-1)/2}$, the network $\mathcal{L}(\mathbf{A}_i)$ is generated by sampling its edges $\mathcal{L}(\mathbf{A}_i)_l$, $l = 1, \dots, V(V-1)/2$ from conditionally independent Bernoulli variables with $\pi_l^{(h)} \in (0, 1)$ defining the probability of a connection among the pair of brain regions indexed by l for $l = 1, \dots, V(V-1)/2$. According to Figure 2, the dependence on the creativity groups is introduced in the latent class assignment mechanism via group-specific mixing probabilities, so that brain networks in the same class share a common edge probability vector $\boldsymbol{\pi}^{(h)}$, with the probability assigned to each class changing across the different groups.

Although massively reducing the number of parameters from $K\{2^{V(V-1)/2} - 1\}$ to $H\{K + V(V-1)/2\} - K$, the choice of modeling separately the connection probabilities in $\boldsymbol{\pi}^{(h)}$ in (2.2) provides a sub-optimal formulation, which does not explicitly account for the network structure of the brain interconnections. For example if region v has a high probability of connection with both regions u and w , this information might provide insights into the connectivity behavior among u and w . Hence, focusing on the l th pair of brain regions, corresponding to nodes v and u , $v > u$, we further reduce the dimensionality of the problem and explicitly borrow information within the brain network by mapping each $\pi_l^{(h)}$, $h = 1, \dots, H$ into a class-specific latent similarity measure $S_l^{(h)} = \log\{\pi_l^{(h)}/(1 - \pi_l^{(h)})\} \in \mathfrak{R}$ via the logistic distribution function, with this latent

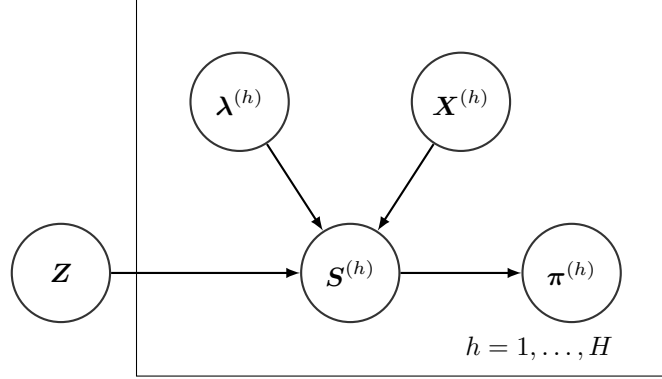


Figure 3: Graphical representation of the mixture representation defined in (2.3) for the class-specific edge probability vectors $\pi^{(h)}$, $h = 1, \dots, H$.

similarity measure further factorized as

$$S_l^{(h)} = Z_l + D_l^{(h)}, \quad D_l^{(h)} = \sum_{r=1}^R \lambda_r^{(h)} X_{vr}^{(h)} X_{ur}^{(h)}, \quad (2.3)$$

for each $l = 1, \dots, V(V-1)/2$ and $h = 1, \dots, H$.

Representation (2.3) separates shared from class-specific components of variability in the brain connectivity structure, with $Z_l \in \mathfrak{R}$ a latent similarity measure for the l th pair of regions common to all individuals and $D_l^{(h)} \in \mathfrak{R}$ a class-specific deviation. Here Z_l is left unstructured as it can be estimated borrowing information across all individuals, while $D_l^{(h)}$ is modeled via a low-rank matrix factorization, exploiting the network structure to cope with less information in the data about class-specific deviations. This is accomplished by embedding the brain regions in a class-specific R -dimensional latent space, with the location of each brain region in the latent space denoted by a vector of latent coordinates $\mathbf{X}_v^{(h)} = (X_{v1}^{(h)}, \dots, X_{vR}^{(h)})^T$, where $X_{vr}^{(h)}$ represents the r th coordinate of region v in class h . According to (2.3) brain regions with coordinates in the same (or opposite) directions have a higher similarity (or dissimilarity) in class h , with the non-negative parameter $\lambda_r^{(h)}$, $r = 1, \dots, R$ measuring the contribution of the r th coordinate in constructing $D_l^{(h)}$. Values $\lambda_r^{(h)} \approx 0$ limit the effect of the corresponding r th coordinate and favor the deletion of redundant dimensions of the latent space. Hence, the connectivity structure in each class is defined by the latent positions, with the parameters $\lambda_r^{(h)}$ measuring the importance of each dimension. Refer to Figure 3 for a graphical representation of factorization (2.3).

We could have considered more complicated scenarios with group dependence introduced also in $\pi^{(h)}$, and in the quantities in (2.3). However, including group dependence only in the mixing probabilities induces further dimensionality reduction, while favoring borrowing of information across the groups in modeling $\pi^{(h)}$, $h = 1, \dots, H$ and provides

simpler testing procedures. Moreover, as stated in Lemma 2.1, such a representation is sufficiently flexible to fully characterize the collection of group-dependent pmfs $\mathbf{p}_{\mathcal{L}(\mathcal{A})|y}$, $y = 1, \dots, K$.

Lemma 2.1. *Any collection of group-dependent probability mass functions $\mathbf{p}_{\mathcal{L}(\mathcal{A})|y} \in \mathcal{P}_{|\mathbb{A}_V|}$, $y = 1, \dots, K$ can be characterized as in (2.2) for some H with class-specific edge probability vectors $\boldsymbol{\pi}^{(h)}$, $h = 1, \dots, H$ factorized as in (2.3) for some R .*

This additionally ensures that any joint probability mass function $\mathbf{p}_{\mathcal{Y}, \mathcal{L}(\mathcal{A})}$ for the random variable $\{\mathcal{Y}, \mathcal{L}(\mathcal{A})\}$ admits representation (2.1)–(2.3) and hence our formulation can be viewed as nonparametric given sufficiently flexible priors for the components.

2.2 Testing for group differences in network data

Factorizations (2.1) and (2.2) facilitate testing of the global association between $\mathcal{L}(\mathcal{A})$ and \mathcal{Y} . Under factorization (2.1), the hypotheses of interest, $H_0 : \mathbf{p}_{\mathcal{Y}, \mathcal{L}(\mathcal{A})} = \mathbf{p}_{\mathcal{Y}} \mathbf{p}_{\mathcal{L}(\mathcal{A})}$ versus $H_1 : \mathbf{p}_{\mathcal{Y}, \mathcal{L}(\mathcal{A})} \neq \mathbf{p}_{\mathcal{Y}} \mathbf{p}_{\mathcal{L}(\mathcal{A})}$, coincide with assessing whether the conditional pmf of the network-valued random variable remains equal $H_0 : p_{\mathcal{L}(\mathcal{A})|1} = \dots = p_{\mathcal{L}(\mathcal{A})|K} = p_{\mathcal{L}(\mathcal{A})}$ or shifts across the groups $H_1 : p_{\mathcal{L}(\mathcal{A})|y} \neq p_{\mathcal{L}(\mathcal{A})|y'}$ for some $y, y' \in \mathbb{Y}$. The characterization of $\mathbf{p}_{\mathcal{L}(\mathcal{A})|y}$ in (2.2) further simplifies the previous systems to testing equality of the mixing probabilities

$$H_0 : \nu_{h1} = \dots = \nu_{hK} \quad \text{versus} \quad H_1 : \nu_{hy} \neq \nu_{hy'} \quad \text{for some } y, y' \in \mathbb{Y}, \quad h = 1, \dots, H. \quad (2.4)$$

This massively reduces the number of parameters to test from $K\{2^{V(V-1)/2} - 1\}$ to $K\{H - 1\}$, with the shared dependence on the common set of node-specific latent coordinates induced by (2.3) preserving the dependence structure within the network also under H_0 . Additionally, recalling Lemma 2.1, under our formulation the system (2.4) uniquely characterizes $H_0 : \mathbf{p}_{\mathcal{Y}, \mathcal{L}(\mathcal{A})} = \mathbf{p}_{\mathcal{Y}} \mathbf{p}_{\mathcal{L}(\mathcal{A})}$ versus $H_1 : \mathbf{p}_{\mathcal{Y}, \mathcal{L}(\mathcal{A})} \neq \mathbf{p}_{\mathcal{Y}} \mathbf{p}_{\mathcal{L}(\mathcal{A})}$.

Recalling our neuroscience application, rejection of H_0 implies that there are differences in brain architecture across creativity groups, but fails to provide insights on which connections are responsible for such global variations. The global differences may be attributable to variations in all brain connections, but more likely there are changes in specific circuits. To obtain further insights, we consider local tests to learn whether each brain connection $\mathcal{L}(\mathcal{A})_l \in \{0, 1\}$ has no association with \mathcal{Y} , $H_{0l} : \mathbf{p}_{\mathcal{Y}, \mathcal{L}(\mathcal{A})_l} = \mathbf{p}_{\mathcal{Y}} \mathbf{p}_{\mathcal{L}(\mathcal{A})_l}$, or differs across low and high creativity subjects, $H_{1l} : \mathbf{p}_{\mathcal{Y}, \mathcal{L}(\mathcal{A})_l} \neq \mathbf{p}_{\mathcal{Y}} \mathbf{p}_{\mathcal{L}(\mathcal{A})_l}$, with $p_{\mathcal{Y}, \mathcal{L}(\mathcal{A})_l}(y, a_l) = \Pr\{\mathcal{Y} = y, \mathcal{L}(\mathcal{A})_l = a_l\}$ and $p_{\mathcal{L}(\mathcal{A})_l}(a_l) = \Pr\{\mathcal{L}(\mathcal{A})_l = a_l\}$, $l = 1, \dots, V(V-1)/2$, $a_l \in \{0, 1\}$. To conduct inference, we measure the association between $\mathcal{L}(\mathcal{A})_l$ and \mathcal{Y} exploiting the model-based version of Cramer's V, proposed in Dunson and Xing (2009), obtaining

$$\begin{aligned} \rho_l^2 &= \frac{1}{\min\{K, 2\} - 1} \sum_{y=1}^K \sum_{a_l=0}^1 \frac{\{p_{\mathcal{Y}, \mathcal{L}(\mathcal{A})_l}(y, a_l) - p_{\mathcal{Y}}(y)p_{\mathcal{L}(\mathcal{A})_l}(a_l)\}^2}{p_{\mathcal{Y}}(y)p_{\mathcal{L}(\mathcal{A})_l}(a_l)} \\ &= \frac{1}{\min\{K, 2\} - 1} \sum_{y=1}^K \sum_{a_l=0}^1 \frac{\{p_{\mathcal{Y}}(y)p_{\mathcal{L}(\mathcal{A})_l|y}(a_l) - p_{\mathcal{Y}}(y)p_{\mathcal{L}(\mathcal{A})_l}(a_l)\}^2}{p_{\mathcal{Y}}(y)p_{\mathcal{L}(\mathcal{A})_l}(a_l)} \end{aligned}$$

$$= \frac{1}{\min\{K, 2\} - 1} \sum_{y=1}^K p_{\mathcal{Y}}(y) \sum_{a_l=0}^1 \frac{\{p_{\mathcal{L}(\mathcal{A})_l|y}(a_l) - p_{\mathcal{L}(\mathcal{A})_l}(a_l)\}^2}{p_{\mathcal{L}(\mathcal{A})_l}(a_l)}. \quad (2.5)$$

Measuring the local association with $\rho_l \in (0, 1)$ provides an appealing choice in terms of interpretation, with $\rho_l = 0$ meaning that $\mathbf{p}_{\mathcal{Y}, \mathcal{L}(\mathcal{A})_l} = \mathbf{p}_{\mathcal{Y}} \mathbf{p}_{\mathcal{L}(\mathcal{A})_l}$, and hence the random variable $\mathcal{L}(\mathcal{A})_l$ modeling the presence or absence of an edge among the l th pair of nodes, has no differences across groups. Additionally, as stated in Lemma 2.2, each ρ_l , $l = 1, \dots, V(V-1)/2$, can be easily computed from the quantities in our model.

Lemma 2.2. *Based on factorizations (2.1) and (2.2), $p_{\mathcal{L}(\mathcal{A})_l|y}(1) = 1 - p_{\mathcal{L}(\mathcal{A})_l|y}(0) = \sum_{h=1}^H \nu_{hy} \pi_l^{(h)}$, and $p_{\mathcal{L}(\mathcal{A})_l}(1) = 1 - p_{\mathcal{L}(\mathcal{A})_l}(0) = \sum_{y=1}^K p_{\mathcal{Y}}(y) \sum_{h=1}^H \nu_{hy} \pi_l^{(h)}$.*

3 Prior specification and posterior computation

3.1 Prior specification and properties

We specify independent priors for the quantities $\mathbf{p}_{\mathcal{Y}} \sim \Pi_{\mathcal{Y}}$, $\mathbf{Z} = (Z_1, \dots, Z_{V(V-1)/2})^T \sim \Pi_{\mathcal{Z}}$, $\mathbf{X}^{(h)} = (X_1^{(h)}, \dots, X_V^{(h)})^T \sim \Pi_{\mathbf{X}}$, $\boldsymbol{\lambda}^{(h)} = (\lambda_1^{(h)}, \dots, \lambda_R^{(h)})^T \sim \Pi_{\boldsymbol{\lambda}}$, $h = 1, \dots, H$ and $\boldsymbol{\nu}_y = (\nu_{1y}, \dots, \nu_{Hy})^T \sim \Pi_{\boldsymbol{\nu}}$, $y = 1, \dots, K$, to induce a prior Π on the joint pmf $\mathbf{p}_{\mathcal{Y}, \mathcal{L}(\mathcal{A})}$ with full support over the $K \times |\mathbb{A}_V|$ dimensional simplex $\mathcal{P}_{K \times |\mathbb{A}_V|}$, while obtaining desirable asymptotic behavior, simple posterior computation and allowance for testing.

As $\mathbf{p}_{\mathcal{Y}}$ is the pmf of a categorical random variable with K levels, we simply let $\{p_{\mathcal{Y}}(1), \dots, p_{\mathcal{Y}}(K)\}^T \sim \text{Dir}(a_1, \dots, a_K)$, and consider the same prior specification suggested by Durante et al. (2015) for the quantities in (2.3) by choosing Gaussian priors for the entries in \mathbf{Z} , standard Gaussians for the elements in $\mathbf{X}^{(h)}$ and multiplicative inverse gammas for $\boldsymbol{\lambda}^{(h)} \sim \text{MIG}(a_1, a_2)$, $h = 1, \dots, H$. This choice for $\Pi_{\boldsymbol{\lambda}}$ favors shrinkage effects with elements in $\boldsymbol{\lambda}^{(h)}$ stochastically decreasing towards 0 as r increases, so as to shrink towards lower dimensional representations and adaptively penalize high dimensional ones. A key of our prior specification is incorporation of global hypothesis testing (2.4) in the definition of $\Pi_{\boldsymbol{\nu}}$. Specifically letting $\mathbf{u} = (u_1, \dots, u_H)^T$ and $\mathbf{u}_y = (u_{1y}, \dots, u_{Hy})^T$, we induce $\Pi_{\boldsymbol{\nu}}$ through

$$\begin{aligned} \boldsymbol{\nu}_y &= (1 - T)\mathbf{u} + T\mathbf{u}_y, \quad y = 1, \dots, K, \\ \mathbf{u} &\sim \text{Dir}(a_1, \dots, a_H), \quad \mathbf{u}_y \sim \text{Dir}(a_1, \dots, a_H), \quad y = 1, \dots, K, \\ T &\sim \text{Bern}\{\text{Pr}(H_1)\}. \end{aligned} \quad (3.1)$$

In (3.1), T is a hypothesis indicator, with $T = 0$ for H_0 and $T = 1$ for H_1 . Under H_1 , we generate group-specific mixing weights independently, while under H_0 we have equal weight vectors. By choosing small values for the hyperparameters in the Dirichlet priors, we favor automatic deletion of redundant classes (Rousseau and Mengersen, 2011). In assessing evidence in favor of the alternative, we can rely on the posterior probability, $\text{Pr}[H_1 | \{\mathbf{y}, \mathcal{L}(\mathcal{A})\}] = 1 - \text{Pr}[H_0 | \{\mathbf{y}, \mathcal{L}(\mathcal{A})\}]$ which can be easily obtained from the output of the Gibbs sampler proposed below. Specifically, under our prior specification,

the full conditional $\Pr(T = 0 \mid -) = \Pr(H_0 \mid -) = 1 - \Pr(H_1 \mid -)$ is analytically available as in Lemma 3.1.

Lemma 3.1. *According to prior specification in (3.1) the full conditional probability $\Pr(T = 0 \mid -)$ of H_0 is*

$$\begin{aligned}
&= \frac{\Pr(H_0) \int \{\prod_{i=1}^n \Pr(G_i \mid \mathbf{u})\} d\Pi_{\mathbf{u}}}{\Pr(H_0) \int \{\prod_{i=1}^n \Pr(G_i \mid \mathbf{u})\} d\Pi_{\mathbf{u}} + \Pr(H_1) \prod_{y=1}^K \int \{\prod_{i:y_i=y} \Pr(G_i \mid \mathbf{u}_y, y_i)\} d\Pi_{\mathbf{u}_y}}, \\
&= \frac{\Pr(H_0) \int (\prod_{h=1}^H u_h^{n_h}) d\Pi_{\mathbf{u}}}{\Pr(H_0) \int (\prod_{h=1}^H u_h^{n_h}) d\Pi_{\mathbf{u}} + \Pr(H_1) \prod_{y=1}^K \int (\prod_{h=1}^H u_{hy}^{n_{hy}}) d\Pi_{\mathbf{u}_y}}, \\
&= \frac{\Pr(H_0) B(\mathbf{a} + \bar{\mathbf{n}}) / B(\mathbf{a})}{\Pr(H_0) B(\mathbf{a} + \bar{\mathbf{n}}) / B(\mathbf{a}) + \Pr(H_1) \prod_{y=1}^K B(\mathbf{a} + \bar{\mathbf{n}}_y) / B(\mathbf{a})}, \tag{3.2}
\end{aligned}$$

with $n_h = \sum_{i=1}^n I(G_i = h)$, $n_{hy} = \sum_{i:y_i=y} I(G_i = h)$, $\mathbf{a} = (a_1, \dots, a_H)^T$, $\bar{\mathbf{n}} = (n_1, \dots, n_H)^T$, $\bar{\mathbf{n}}_y = (n_{1y}, \dots, n_{Hy})^T$ and B indicates the multivariate Beta function $B(\mathbf{x}) = \prod_{i=1}^q \Gamma(x_i) / \Gamma(\sum_{i=1}^q x_i)$ with $\Gamma(x_i)$ the Gamma function.

Although providing a key choice for performing global testing, it is impractical to adopt formulation (3.1) for each local point null $H_{0l} : \rho_l = 0$ versus $H_{1l} : \rho_l \neq 0$, $l = 1, \dots, V(V-1)/2$. Hence, we replace local point nulls with small interval nulls $H_{0l} : \rho_l \leq \epsilon$ versus $H_{1l} : \rho_l > \epsilon$. This choice allows $\Pr[H_{1l} \mid \{\mathbf{y}, \mathcal{L}(\mathbf{A})\}] = 1 - \Pr[H_{0l} \mid \{\mathbf{y}, \mathcal{L}(\mathbf{A})\}]$ to be easily estimated as the proportion of Gibbs samples in which $\rho_l > \epsilon$. Moreover, as noted in Berger and Sellke (1987) the small interval hypothesis $H_{0l} : \rho_l \leq \epsilon$ can be realistically approximated by $H_{0l} : \rho_l = 0$.

Beside key computational properties, as stated in Lemma 3.2, our choices induce a prior Π for $\mathbf{p}_{\mathcal{Y}, \mathcal{L}(\mathbf{A})}$ with full L_1 support over $\mathcal{P}_{K \times |\mathbb{A}_V|}$, meaning that Π can generate a $\mathbf{p}_{\mathcal{Y}, \mathcal{L}(\mathbf{A})}$ within an arbitrarily small L_1 neighborhood of the true data-generating model $\mathbf{p}_{\mathcal{Y}, \mathcal{L}(\mathbf{A})}^0$, allowing the truth to fall in a wide class.

Lemma 3.2. *Based on the priors $\Pi_y, \Pi_Z, \Pi_X, \Pi_\lambda$, and Π_ν , and letting $B_\epsilon(\mathbf{p}_{\mathcal{Y}, \mathcal{L}(\mathbf{A})}^0) = \{\mathbf{p}_{\mathcal{Y}, \mathcal{L}(\mathbf{A})} : \sum_{y=1}^K \sum_{\mathbf{a} \in \mathbb{A}_V} |p_{\mathcal{Y}, \mathcal{L}(\mathbf{A})}(y, \mathbf{a}) - p_{\mathcal{Y}, \mathcal{L}(\mathbf{A})}^0(y, \mathbf{a})| < \epsilon\}$ denote the L_1 neighborhood around $\mathbf{p}_{\mathcal{Y}, \mathcal{L}(\mathbf{A})}^0$, then for any $\mathbf{p}_{\mathcal{Y}, \mathcal{L}(\mathbf{A})}^0 \in \mathcal{P}_{K \times |\mathbb{A}_V|}$ and $\epsilon > 0$, $\Pi\{B_\epsilon(\mathbf{p}_{\mathcal{Y}, \mathcal{L}(\mathbf{A})}^0)\} > 0$.*

This is a key property to ensure good performance in our application because without prior support about the true data-generating pmf, the posterior cannot possibly concentrate around the truth. Moreover, as $\mathbf{p}_{\mathcal{Y}, \mathcal{L}(\mathbf{A})}$ is characterized by finitely many parameters $p_{\mathcal{Y}, \mathcal{L}(\mathbf{A})}(y, \mathbf{a})$, $y \in \mathbb{Y}$, $\mathbf{a} \in \mathbb{A}_V$, Lemma 3.2 is sufficient to guarantee that the posterior assigns probability one to any arbitrarily small neighborhood of the true joint pmf as the number of observations $n \rightarrow \infty$, meaning that $\Pi[B_\epsilon(\mathbf{p}_{\mathcal{Y}, \mathcal{L}(\mathbf{A})}^0) \mid \{y_1, \mathcal{L}(\mathbf{A}_1)\}, \dots, \{y_n, \mathcal{L}(\mathbf{A}_n)\}]$ converges almost surely to 1, when $\mathbf{p}_{\mathcal{Y}, \mathcal{L}(\mathbf{A})}^0$ is the true joint pmf.

3.2 Posterior computation

Posterior computation is available via the following simple and efficient Gibbs sampler.

1. Sample \mathbf{p}_y from the full conditional $\{p_y(1), \dots, p_y(K)\}^T \mid - \sim \text{Dir}(a_1+n_1, \dots, a_K+n_K)$, with $n_y = \sum_{i=1}^n \mathbf{I}(y_i = y)$.
2. For $i = 1, \dots, n$, update G_i from the multinomial with probabilities

$$\Pr(G_i = h \mid -) = \frac{\nu_{hy_i} \prod_{l=1}^{V(V-1)/2} \{\pi_l^{(h)}\}^{\mathcal{L}(A_i)_l} \{1 - \pi_l^{(h)}\}^{1-\mathcal{L}(A_i)_l}}{\sum_{m=1}^H \nu_{my_i} \prod_{l=1}^{V(V-1)/2} \{\pi_l^{(m)}\}^{\mathcal{L}(A_i)_l} \{1 - \pi_l^{(m)}\}^{1-\mathcal{L}(A_i)_l}}.$$

3. Given $G_i, i = 1, \dots, n$, the updating for quantities $\mathbf{Z}, \mathbf{X}^{(h)}$ and $\boldsymbol{\lambda}^{(h)}, h = 1, \dots, H$ proceeds via the recently developed Polyá-gamma data augmentation scheme for Bayesian logistic regression (Polson et al., 2013) as in Durante et al. (2015).
4. Sample the testing indicator T from the full conditional Bernoulli with probability (3.2).
5. If $T = 0$, let $\boldsymbol{\nu}_y = \mathbf{u}, y = 1, \dots, K$ with \mathbf{u} updated from the full conditional Dirichlet $(u_1, \dots, u_H)^T \mid - \sim \text{Dir}(a_1 + n_1, \dots, a_H + n_H)$. Otherwise, if $T = 1$, update each $\boldsymbol{\nu}_y$ independently from $(\nu_{1y}, \dots, \nu_{Hy})^T \mid - \sim \text{Dir}(a_1 + n_{1y}, \dots, a_H + n_{Hy})$.

Since the number of mixing components in (2.2) and the dimensions of the latent spaces in (2.3) are not known in practice, we perform posterior computation by fixing H and R at conservative upper bounds. The priors are chosen to allow adaptive emptying of the redundant components, with the posteriors for parameters controlling unnecessary dimensions concentrated near zero. If all the classes h are occupied, then H should be increased. Similarly, if the posterior for $\lambda_R^{(h)}$ is not concentrated near zero for any h , then R should be increased.

4 Simulation studies

We consider simulation studies to evaluate the performance of our method in accurately estimating the joint pmf for the pair $\{\mathcal{Y}, \mathcal{L}(\mathcal{A})\}$, in correctly assessing the global hypothesis of association among the network-valued random variable and the categorical predictor, and in identifying local variations in each edge probability across groups.

For comparison we also implement a MANOVA procedure (see e.g. Krzanowski, 1988) to test for global variations across groups of the random vector Θ of summary measures, with realization $\boldsymbol{\theta}_i$ of Θ comprising the most commonly used topological summary statistics (e.g. density in the whole network, density in nodes blocks, averaged shortest path length, clustering coefficient) computed for each network i ; see Kantarci and Labatut (2013) for an overview on these topological network measures. For local testing, we compare our procedure to the results obtained when testing on the association between $\mathcal{L}(\mathcal{A})_l$ and \mathcal{Y} for each $l = 1, \dots, V(V-1)/2$ via separate two-sided Fisher's exact tests (see e.g. Agresti, 2002). We consider exact tests to avoid issues arising from the χ^2 approximations in sparse tables.

We simulate $n = 50$ pairs (y_i, \mathbf{A}_i) from our model (2.1)–(2.3), with y_i from a categorical variable having two equally likely groups $\mathbf{p}_y^0 = (0.5, 0.5)^T$ and \mathbf{A}_i a $V \times V$ network with $V = 20$ nodes. We consider $H = 2$ latent classes, with $\boldsymbol{\pi}^{0(h)}$ defined as in (2.3). Brain networks are typically characterized by tighter intra-hemispheric than inter-hemispheric connections (Roncal et al., 2013). Hence, we consider two node blocks $\{1, \dots, 10\}$ and $\{11, \dots, 20\}$, and generate entries in \mathbf{Z}^0 to favor more likely connections between pairs in the same block than pairs in different blocks. To assess the local testing performance, we induce group differences only on a subset of nodes $V^* \subset V$. A possibility to favor this behavior is to let $R = 1$, $\lambda^{0(1)} = \lambda^{0(2)} = 1$ and generate $X_v^{0(h)}$ from independent standard Gaussians for all $v \in V^*$, while fixing the latent coordinates of the remaining nodes to 0. As a result, no variations in edge probabilities are displayed when mixing probabilities remain constant, while only local differences are highlighted when mixing probabilities shift across groups. Under the dependence scenario, data are simulated with group-specific mixing probabilities $\boldsymbol{\nu}_1^0 = (0.8, 0.2)^T$, $\boldsymbol{\nu}_2^0 = (0.2, 0.8)^T$. Instead, constant mixing probabilities $\boldsymbol{\nu}_1^0 = \boldsymbol{\nu}_2^0 = (0.5, 0.5)^T$ are considered under independence. Although we focus only on 20 nodes to facilitate graphical analyses, the mixture representation in (2.2) and the low-rank factorization in (2.3) scale to much higher V settings.

In both scenarios, inference is accomplished by considering $H = R = 10$, $\Pr(H_1) = \Pr(H_0) = 0.5$ and letting $\mathbf{p}_y \sim \text{Dir}(1/2, 1/2)$. To favor deletion of unnecessary classes h , we fix the hyperparameter vector in the Dirichlet for \mathbf{u} and \mathbf{u}_y to $\mathbf{a} = (a_1 = 1/H, \dots, a_H = 1/H)^T$. As noted in Ishwaran and Zarepour (2002), this choice provides also a finite approximation to the Dirichlet Process. For priors Π_Z, Π_X and Π_λ , we choose the same hyperparameter settings suggested by Durante et al. (2015). We collect 5,000 Gibbs iterations, discarding the first 1,000. In both scenarios mixing was assessed via effective sample sizes for the quantities of interest for inference covering the group-specific edge probability vectors $\bar{\boldsymbol{\pi}}_y$, with elements $\bar{\pi}_{yl} = \Pr\{\mathcal{L}(\mathcal{A})_l = 1 \mid \mathcal{Y} = y\} = \sum_{h=1}^H \nu_{hy} \pi_l^{(h)}$ according to Lemma 2.2. This vector coincides with the group-specific mean network structure $\mathbb{E}\{\mathcal{L}(\mathcal{A}) \mid \mathcal{Y} = y\} = \sum_{\mathbf{a} \in \mathbb{A}_V} \mathbf{a} \times p_{\mathcal{L}(\mathcal{A})|y}(\mathbf{a}) = \sum_{h=1}^H \nu_{hy} \boldsymbol{\pi}^{(h)}$ under factorization (2.2). In both scenarios, most of the effective samples sizes are $\approx 2,000$ out of 4,000 samples, demonstrating excellent mixing performance.

Our testing procedure allows accurate inference on the global association between $\mathcal{L}(\mathcal{A})$ and \mathcal{Y} . We obtain $\hat{\Pr}[H_1 \mid \{\mathbf{y}, \mathcal{L}(\mathcal{A})\}] > 0.99$ for the association scenario and $\hat{\Pr}[H_1 \mid \{\mathbf{y}, \mathcal{L}(\mathcal{A})\}] < 0.01$ when y_i and \mathbf{A}_i , $i = 1, \dots, n$ are generated independently. Instead, the MANOVA testing procedure on the summary statistics vector favors the hypothesis of no association in both scenarios at a level $\alpha = 0.1$. This result further highlights how global network measures may fail in accurately characterizing the whole network architecture. We obtain similarly good performance in correctly recovering the true pmf for $\{\mathcal{Y}, \mathcal{L}(\mathcal{A})\}$ under both scenarios. This is highlighted in Figures 4–5 summarizing the posterior distribution of the key quantities, which define the joint pmf through (2.1) and (2.2). As Figures 4 and 5 provide inference on class-specific quantities, we additionally accounted for label switching via the Stephens (2000) relabeling algorithm. However, no relabeling was necessary in our simulations.

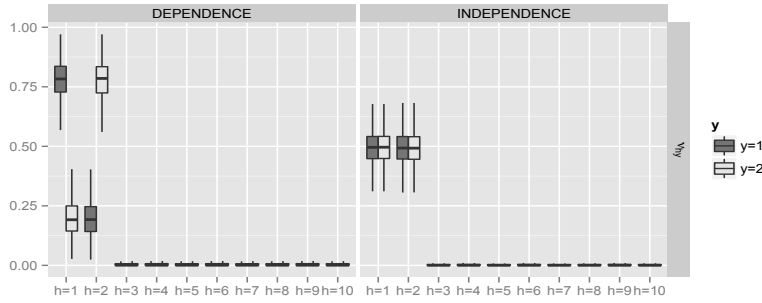


Figure 4: Boxplots constructed using posterior samples of the group-specific mixing probabilities in the dependence and independence scenarios.

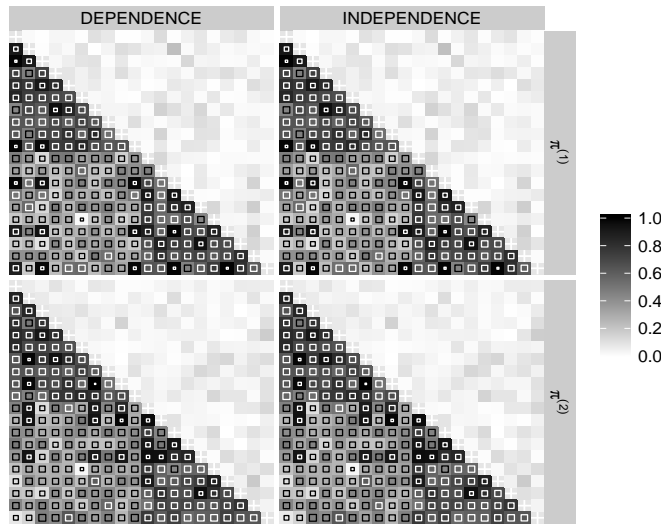


Figure 5: For the same scenarios, posterior mean of $\pi^{(h)}$, for the two non-empty classes $h = 1, 2$ (lower triangular), and posterior mean of the absolute value of $\pi^{(h)} - \pi^{0(h)}$ (upper triangular). Squares dimensions are proportional to the length of the 95% highest posterior density intervals.

As expected we learn posterior distributions for the mixing probabilities which shift over the grouping variable or remain constant under dependence and independence, respectively, as shown in Figure 4. Note also how the sparse Dirichlet priors for quantities \mathbf{u} and \mathbf{u}_y allow us to efficiently remove redundant dimensions. Borrowing of information across the groups provides accurate estimates of the class-specific edge probability vectors $\pi^{(h)}$, with posterior distribution concentrated around the true values, as con-

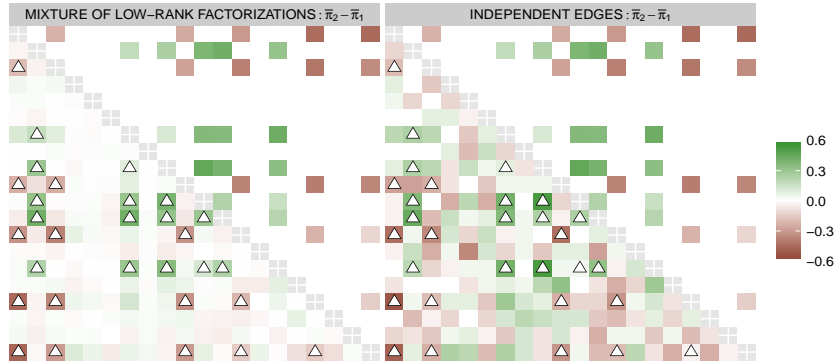


Figure 6: Lower Triangular: posterior mean of the difference between the edge probability vectors in the two groups under our model (left) and maximum likelihood estimate of this difference when considering each pair of nodes separately (right). Upper Triangular: true differences. Triangles highlight edges which differ across groups in the true process.

firmed in Figure 5. We obtain similar performance in estimating \mathbf{p}_Y , with the posterior concentrated around the true \mathbf{p}_Y^0 .

Focusing on the dependence scenario, Figure 6 shows how accounting for sparsity and network information, via our dependent mixture of low-rank factorizations, provides good estimates of local variations in edge probabilities, correctly highlighting pairs of nodes whose connectivity differs across groups in the true generating process. Conducting inference on each pair of nodes separately provides instead poor estimates, with the sub-optimality arising from inefficient borrowing of information across the edges. This lack of efficiency strongly affects also the local testing performance as shown in Figure 7, with our procedure having higher power than the one obtained via separate Fisher’s exact tests. In Figure 7, each Fisher’s exact test p-value is transformed via $1/(1 - ep_l \log p_l)$ if $p_l < 1/e$ and 0.5 otherwise, to allow better comparison with $\hat{\Pr}[H_{1l} | \{\mathbf{y}, \mathcal{L}(\mathbf{A})\}]$ (Selke et al., 2001). Moreover, we adjust for multiplicity in the Fisher’s exact tests by rejecting all those pairs having a p-value below p^* , with p^* the Benjamini and Hochberg (1995) threshold to maintain a false discovery rate $\text{FDR} \leq 0.1$. To maintain a similar rejection region in the two procedures we reject all l with $\hat{\Pr}[H_{1l} | \{\mathbf{y}, \mathcal{L}(\mathbf{A})\}] > p^{**}$, $p^{**} = 1/(1 - ep^* \log p^*)$ if $p^* < 1/e$, 0.5 otherwise, under our local Bayesian testing.

To assess frequentist operating characteristics, we repeated the above simulation exercise for 100 simulated datasets under both dependence and independence scenarios. The MANOVA test is performed under a threshold $\alpha = 0.1$, while the decision rule in the local Fisher’s exact tests is based on the Benjamini and Hochberg (1995) threshold to maintain a false discovery rate $\text{FDR} \leq 0.1$. Under our Bayesian procedure we reject the global null if $\hat{\Pr}[H_{1l} | \{\mathbf{y}, \mathcal{L}(\mathbf{A})\}] > 1 - \alpha^*$ with $\alpha^* = \{1 + (-e\alpha \log \alpha)^{-1}\}^{-1}$ to provide comparable decision rules with the frequentist MANOVA test at a level $\alpha = 0.1$. Our local testing procedure contains an intrinsic Bayesian adjustment for multiple testing, so

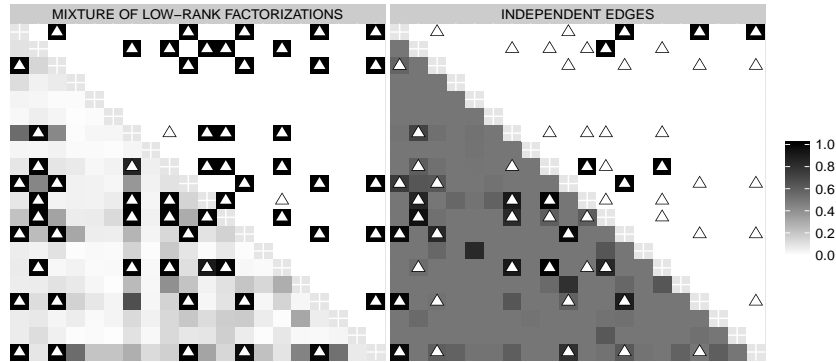


Figure 7: Lower Triangular: $\hat{\Pr}[H_{1l} | \{\mathbf{y}, \mathcal{L}(\mathbf{A})\}] = \Pr[\rho_l > 0.1 | \{\mathbf{y}, \mathcal{L}(\mathbf{A})\}]$ (left) and calibrated Fisher's exact tests p-values $1/(1 - e p_l \log p_l)$ if $p_l < 1/e$, 0.5 otherwise, to allow comparison with $\hat{\Pr}[H_{1l} | \{\mathbf{y}, \mathcal{L}(\mathbf{A})\}]$ (right). Upper Triangular: Accepted (white) and rejected (black) local hypotheses.

	Type I error	Type II error	FWER	FDR
Global testing procedure				
Mixture of low-rank factorizations	0.01	0.01		
MANOVA on summary measures	0.10	0.87		
Local testing procedure				
Mixture of low-rank factorizations	0.0004	0.0587	0.0600	0.0023
Separate Fisher's exact tests	0.0036	0.5983	0.4000	0.0387

Table 1: Comparison of error rates for our procedure against MANOVA on summary statistics for global testing and separate Fisher's exact tests for local hypotheses.

we do not adjust the threshold but instead reject local nulls if $\hat{\Pr}[H_{1l} | \{\mathbf{y}, \mathcal{L}(\mathbf{A})\}] > 0.9$.

Table 1 confirms the superior performance of our approach in maintaining all error rates close to zero, in both global and local testing, while automatically adjusting for multiplicity. The information reduction via summary measures for the global test and the lack of a network structure in the local Fisher's exact tests lead to procedures with substantially less power. Although Table 1 has been constructed using a particular threshold of 0.9 in the local testing procedure, we also have clearly superior performance allowing the thresholds in the local tests to vary obtaining the ROC curves in Figure 8.

In considering sample size versus type I and type II error rates, it is interesting to assess the rate at which the posterior probability of the global alternative $\Pr[H_1 | \{\mathbf{y}, \mathcal{L}(\mathbf{A})\}]$ converges to 0 and 1 under H_0 and H_1 , respectively, as n increases. We evaluate this behavior by simulating 100 datasets as in the previous simulation for increasing sample sizes $n = 20$, $n = 40$ and $n = 100$ and for each scenario. Figure 9 provides the histograms showing the estimated posterior probabilities of H_1 for the 100 simulated datasets under the two scenarios and for increasing sample sizes. The

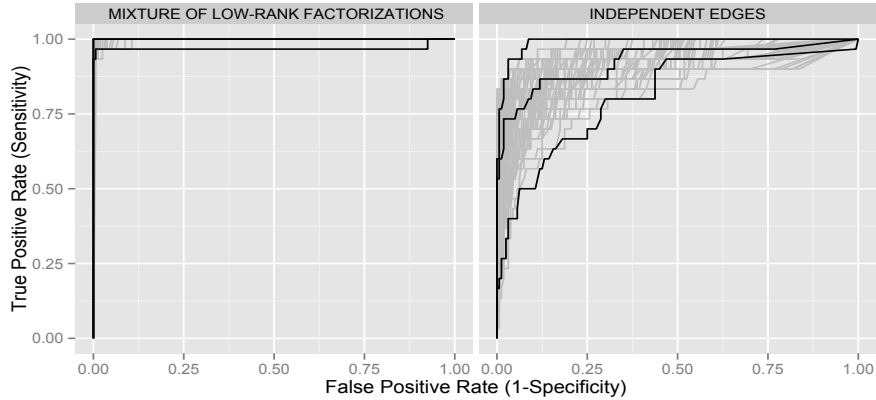


Figure 8: For local testing, ROC curves from each simulation constructed using the true hypotheses indicator vector δ ($\delta_l = 0$ if H_{0l} is true, $\delta_l = 1$ if H_{1l} is true, $l = 1, \dots, V(V-1)/2$) and $\hat{\Pr}[H_{1l} | \{\mathbf{y}, \mathcal{L}(\mathbf{A})\}]$ (left) or $1 - p_l$ with p_l the Fisher's exact p-values (right). We highlight in black the ROC curves having the highest, median and lowest area under the curve.

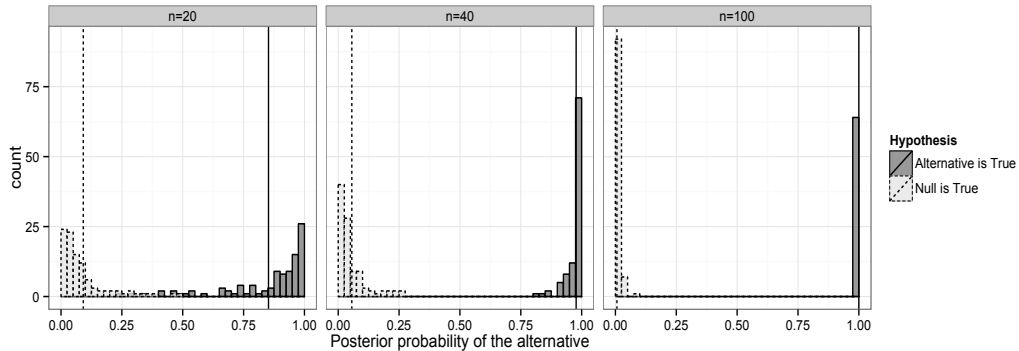


Figure 9: For increasing sample sizes n , histograms of the estimated posterior probabilities of the global alternative H_1 in each of the 100 simulations under association and no association.

separation between scenarios is evident for all sample sizes, with $\hat{\Pr}[H_1 | \{\mathbf{y}, \mathcal{L}(\mathbf{A})\}]$ consistently concentrating around 0 and 1 under the no association and association scenario, respectively, as n increases. When $n = 20$ the test has lower power, with 32/100 samples having $\hat{\Pr}[H_1 | \{\mathbf{y}, \mathcal{L}(\mathbf{A})\}] < 0.9$ when H_1 is true. However, type I errors were rare, with 1/100 samples having $\hat{\Pr}[H_1 | \{\mathbf{y}, \mathcal{L}(\mathbf{A})\}] > 0.9$ when data are generated under H_0 . These values are ≈ 0 when the sample size is increased to $n = 40$ and $n = 100$, with the latter showing strongly concentrated estimates around 1 and 0, when H_1 is true and H_0 is true, respectively.

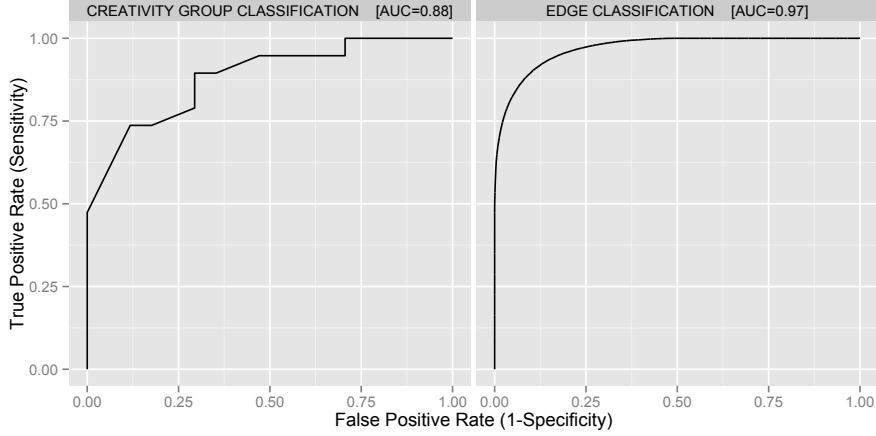


Figure 10: Left: ROC curve constructed using the creativity group y_i , $i = 1, \dots, n$ and its estimated conditional probability from equation (5.1). Right: ROC curve constructed using observed edges $\mathcal{L}(A_i)_l$, $i = 1, \dots, n$, $l = 1, \dots, V(V-1)/2$ and the posterior mean of their group-specific marginal probability $\pi_{il} \mid y_i = \sum_{h=1}^H \nu_{h1} \pi_l^{(h)}$ if i is in the low creativity group ($y_i = 1$) or $\pi_{il} \mid y_i = \sum_{h=1}^H \nu_{h2} \pi_l^{(h)}$ if i is in the high creativity group ($y_i = 2$).

5 Application to human brain networks and creativity

We apply our method to the dataset described in the introduction using the same settings as in the simulation examples, but with upper bound H increased to $H = 15$. This choice proves to be sufficient with classes $h = 12, \dots, 15$ having no observations and redundant dimensions of the latent spaces efficiently removed. The efficiency of the Gibbs sampler was very good, with effective sample sizes $\approx 1,500$ out of 4,000.

Our results provide interesting insights into the global relation between the brain network structure and creativity, with $\hat{\Pr}[H_1 \mid \{\mathbf{y}, \mathcal{L}(\mathbf{A})\}] = 0.995$ strongly favoring the alternative hypothesis of association between brain region interconnections and level of creativity. We also attempted to apply the MANOVA test as implemented in the simulation experiments, with the same network statistics. However, the averaged shortest path length was undefined for three subjects, as there were no paths between several pairs of their brain regions. Replacing these undefined shortest path lengths with the maximum of the finite averaged shortest path lengths, we obtained no significant difference between creativity groups (p-value=0.076). When excluding this topological measure, we instead obtain a borderline significant p-value of 0.046. This sensitivity to the choice of summary statistics further motivates tests that avoid choosing topological measures, which is an inherently arbitrary exercise.

A key of our procedure is in providing efficient dimensionality reduction via mixture modeling and matrix factorization procedures, while preserving general flexibility

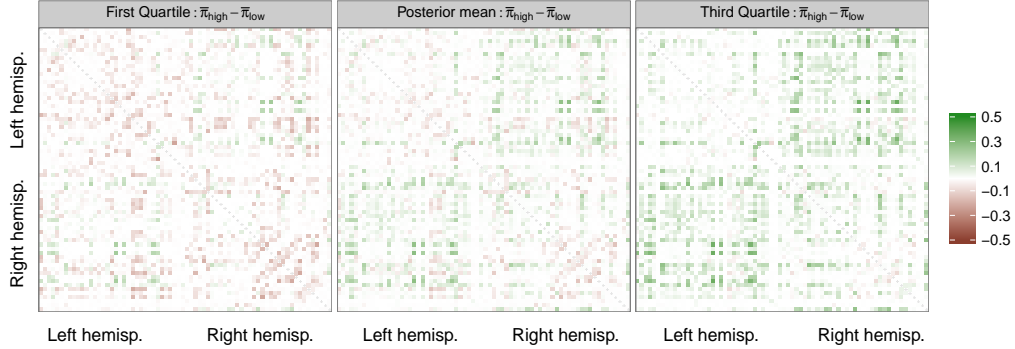


Figure 11: Mean and quartiles for the posterior distribution of the difference between the edge probabilities in high creativity subjects $\bar{\pi}_{high}$ and low creativity subjects $\bar{\pi}_{low}$.

in characterizing replicated network data. This is highlighted in the right plot of Figure 10 showing excellent performance in edge classification based on their group-specific marginal probabilities. Beside providing a flexible approach in joint modeling of networks and categorical predictors, our methodology represents also a powerful and general tool to predict y_i given the subject's full brain network structure. In fact, under our framework, the probability that a subject i has high creativity, conditionally on his brain structural connectivity network \mathbf{A}_i , is simply

$$\begin{aligned} \Pr\{\mathcal{Y} = 2 \mid \mathcal{L}(\mathbf{A}_i)\} &= 1 - \Pr\{\mathcal{Y} = 1 \mid \mathcal{L}(\mathbf{A}_i)\} \\ &= \frac{p_{\mathcal{Y}}(2)p_{\mathcal{L}(\mathcal{A})|y=2}(\mathbf{a}_i)}{p_{\mathcal{Y}}(2)p_{\mathcal{L}(\mathcal{A})|y=2}(\mathbf{a}_i) + p_{\mathcal{Y}}(1)p_{\mathcal{L}(\mathcal{A})|y=1}(\mathbf{a}_i)}, \end{aligned} \quad (5.1)$$

where $\mathbf{a}_i = \mathcal{L}(\mathbf{A}_i)$ is the network configuration of the i th subject and $p_{\mathcal{L}(\mathcal{A})|y}(\mathbf{a}_i)$, ($y = 1, 2$) can be easily computed from (2.2). As shown in the left plot of Figure 10 allowing the conditional pmf of the network-valued random variable to shift across groups via group-specific mixing probabilities provides a good characterization of the dependence between brains and creativity, leading to accurate classification of the creativity group.

Results in Figure 10 confirm the good fit of our model to the data, motivating further analysis and interpretation of the results with respect to available literature. Figure 11 provides summaries of the posterior distribution for $\bar{\pi}_{high} - \bar{\pi}_{low}$, with $\bar{\pi}_{high} = \sum_{h=1}^H \nu_{h2} \boldsymbol{\pi}^{(h)}$ and $\bar{\pi}_{low} = \sum_{h=1}^H \nu_{h1} \boldsymbol{\pi}^{(h)}$ encoding the edge probabilities in high and low creativity groups, respectively, as well as the conditional expectation of the corresponding network-valued random variable. Most of these connections have a similar probability in the two groups, with more evident local differences for connections among brain regions in different hemispheres. Highly creative individuals display a higher propensity to form inter-hemispheric connections. Differences in intra-hemispheric circuits are less evident. These findings are confirmed by Figure 12 including also results from our local testing procedure. The threshold on ρ_l is fixed at $\epsilon = 0.1$ and the decision rule rejects the local nulls when $\Pr[H_{1l} \mid \{\mathbf{y}, \mathcal{L}(\mathbf{A})\}] > 0.9$. These choices

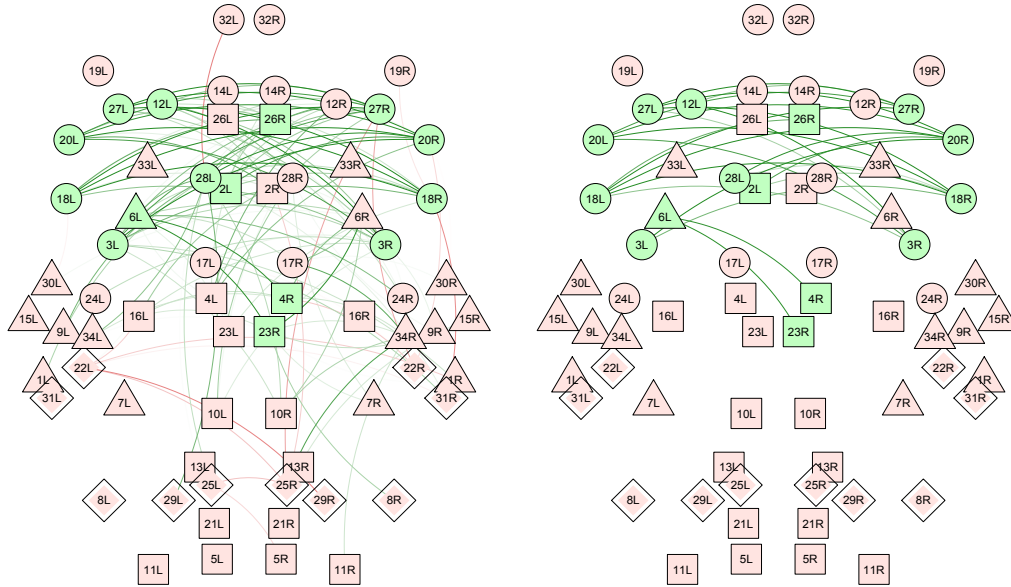


Figure 12: Left: weighted network visualization with weights given by the estimated difference among the edge probabilities in the two creativity groups $\hat{\pi}_{high} - \hat{\pi}_{low}$. Edge colors range from red to green as the corresponding difference goes from -1 to 1 . Right: estimated difference among the edge probabilities in the two groups highlighted only for those connections with $\hat{P}r[H_{il} | \{\mathbf{y}, \mathcal{L}(\mathbf{A})\}] > 0.9$ from our local testing procedure. Frontal lobe regions (circles), Limbic (square), Temporal (triangle), Parietal (diamond), Occipital (rectangle) according to Kang et al. (2012) classification of Desikan atlas in anatomical lobes. Regions are green if they have at least one edge with $\hat{P}r[H_{il} | \{\mathbf{y}, \mathcal{L}(\mathbf{A})\}] > 0.9$, otherwise they are red, and their positions are given by the spatial coordinates in the brain.

provide reasonable settings based on simulations, and results are robust to moderate changes in the thresholds.

Previous studies show that intra-hemispheric connections are more likely than inter-hemispheric connections for healthy individuals (Roncal et al., 2013). This is also evident in our dataset, with subjects having a proportion of intra-hemispheric edges of ≈ 0.55 over the total number of possible intra-hemispheric connections, against a proportion of ≈ 0.21 for the inter-hemispheric ones. Our estimates in Figure 11 and local tests in Figure 12 highlight differences in terms of inter-hemispheric connectivity behavior, with highly creative subjects having a stronger propensity for links between regions in different hemispheres. This is consistent with the idea that creative innovations are a result of communication between brain regions that ordinarily are not strongly connected (Heilman et al., 2003).

These findings contribute to the ongoing debate on the sources of creativity in the

human brain, with original theories considering the right-hemisphere as the seat of creative thinking, and more recent empirical analyses highlighting the importance of the level of communication between the two hemispheres of the brain; see Sawyer (2012), Shobe et al. (2009) and the references cited therein. Beside the different techniques in monitoring brain networks and measuring creativity, as stated in Arden et al. (2010), previous lack of agreement is likely due to the absence of a unifying approach to statistical inference in this field. Our method addresses this issue, while essentially supporting modern theories considering creativity as a result of cooperating hemispheres.

Figure 12 shows how the differences in terms of inter-hemispheric connectivity are found mainly in the frontal lobe, where the co-activation circuits in the high creativity group are denser. This result is in line with recent findings highlighting the major role of the frontal lobe in creative cognition (Carlsson et al., 2000; Jung et al., 2010; Takeuchi et al., 2010). Previous analyses focus on variations in the activity of each region in isolation, with Carlsson et al. (2000) and Takeuchi et al. (2010) inferring an increase in cerebral blood flow and fractional anisotropy, respectively, for highly creative subjects, and Jung et al. (2010) showing a negative association between creativity and cortical thickness in frontal regions. We instead provide inference on interconnections among these regions, with an increase in bilateral frontal connectivity for high creativity subjects, consistent with both the attempt to enhance frontal brain activity as suggested by Carlsson et al. (2000) and Takeuchi et al. (2010) or reduce it according to Jung et al. (2010).

6 Discussion

This article proposes the first approach in the literature (to our knowledge) for inference on group differences in network-valued data without reducing the network data to summary statistics prior to inference. The creativity application illustrates substantial benefits of our approach in providing a unifying and powerful methodology to perform inferences on group differences in brain networks, in sharp contrast to current practice, which applies simple statistical tests based on network topological measures. These tests tend to lack power and be highly sensitive to the features chosen, contributing to the inconsistent results observed in the recent literature. Although we specifically focus on creativity, our method can be applied directly in many other settings. For example, for inferring differences in brain networks with neuropsychiatric disease, gender, intelligence groups, and stimuli. Similarly, our approach is applicable beyond brain networks to other settings involving network-valued data. Interesting ongoing directions include the incorporation of non-categorical response variables and covariates, and accommodation of weighted and frequency-dependent network data.

7 Appendix

Proof. of Lemma 2.1 Recalling Lemma 2.1 in Durante et al. (2015) we can always represent each $p_{\mathcal{L}(\mathcal{A})|y}(\mathbf{a})$, $y = 1, \dots, K$ as $p_{\mathcal{L}(\mathcal{A})|y}(\mathbf{a}) = \sum_{h=1}^{H_y} \nu_{hy}^* \prod_{l=1}^{V(V-1)/2} \{\pi_l^{(hy)}\}^{a_l} \{1 -$

$\pi_l^{(hy)}\}^{1-a_l}$, with each $\pi_l^{(hy)}$ factorized as $\text{logit}\{\pi_l^{(hy)}\} = Z_l^{(y)} + \sum_{r=1}^{R_y} \lambda_r^{(hy)} X_{vr}^{(hy)} X_{ur}^{(hy)}$, $l = 1, \dots, V(V-1)/2$ and $h = 1, \dots, H_y$. Hence Lemma 2.1 follows after choosing $\boldsymbol{\pi}^{(h)}, h = 1, \dots, H$ as the sequence of unique class-specific edge probability vectors $\boldsymbol{\pi}^{(hy)}$ appearing in the previous factorization for at least one group y , and letting the group-specific mixing probabilities in (2.2) be $\nu_{hy} = \nu_{hy}^*$ if $\boldsymbol{\pi}^{(h)} = \boldsymbol{\pi}^{(hy)}$ and $\nu_{hy} = 0$ otherwise. \square

Proof. of Lemma 2.2 Recalling factorization 2.2 and letting \mathbb{A}_V^{-l} the set containing all the possible network configurations for the node pairs except the l -th one, we have that $p_{\mathcal{L}(\mathcal{A})_l|y}(1)$ is equal to

$$\sum_{\mathbb{A}_V^{-l}} \sum_{h=1}^H \nu_{hy} \pi_l^{(h)} \prod_{l^* \neq l} \{\pi_{l^*}^{(h)}\}^{a_{l^*}} \{1 - \pi_{l^*}^{(h)}\}^{1-a_{l^*}} = \sum_{h=1}^H \nu_{hy} \pi_l^{(h)} \sum_{\mathbb{A}_V^{-l}} \prod_{l^* \neq l} \{\pi_{l^*}^{(h)}\}^{a_{l^*}} \{1 - \pi_{l^*}^{(h)}\}^{1-a_{l^*}}$$

Then Lemma 2.2 follows after noticing that $\prod_{l^* \neq l} \{\pi_{l^*}^{(h)}\}^{a_{l^*}} \{1 - \pi_{l^*}^{(h)}\}^{1-a_{l^*}}$ is the joint pmf of independent Bernoulli random variables and hence the summation over the whole joint sample space $\mathbb{A}_V^{-l} = \{0, 1\}^{V(V-1)/2-1}$, provides $\sum_{\mathbb{A}_V^{-l}} \prod_{l^* \neq l} \{\pi_{l^*}^{(h)}\}^{a_{l^*}} \{1 - \pi_{l^*}^{(h)}\}^{1-a_{l^*}} = 1$. The proof for the marginal $p_{\mathcal{L}(\mathcal{A})_l}(1) = \sum_{y=1}^K p_{\mathcal{Y}}(y) \sum_{h=1}^H \nu_{hy} \pi_l^{(h)}$ follows directly from previous result after noticing that $p_{\mathcal{L}(\mathcal{A})_l}(1) = \sum_{y=1}^K p_{\mathcal{Y}, \mathcal{L}(\mathcal{A})_l}(y, 1) = \sum_{y=1}^K p_{\mathcal{Y}}(y) p_{\mathcal{L}(\mathcal{A})_l|y}(1)$. \square

Proof. of Lemma 3.1 To prove Lemma 3.1 we need to show that $\int (\prod_{h=1}^H u_h^{n_h}) d\Pi_{\mathbf{u}} = \text{B}(\mathbf{a} + \bar{\mathbf{n}})/\text{B}(\mathbf{a})$ and $\int (\prod_{h=1}^H u_{hy}^{n_{hy}}) d\Pi_{\mathbf{u}_y} = \text{B}(\mathbf{a} + \bar{\mathbf{n}}_y)/\text{B}(\mathbf{a})$ under the Dirichlet prior for \mathbf{u} and $\mathbf{u}_y, y = 1, \dots, K$ specified in (3.1). Hence

$$\begin{aligned} \int \prod_{h=1}^H u_h^{n_h} d\Pi_{\mathbf{u}} &= \frac{\Gamma(\sum_{h=1}^H a_h)}{\prod_{h=1}^H \Gamma(a_h)} \int \prod_{h=1}^H u_h^{n_h} u_h^{a_h-1} d\mathbf{u} \\ &= \frac{\Gamma(\sum_{h=1}^H a_h)}{\prod_{h=1}^H \Gamma(a_h)} \frac{\prod_{h=1}^H \Gamma(n_h + a_h)}{\Gamma\{\sum_{h=1}^H (n_h + a_h)\}} \int \frac{\Gamma\{\sum_{h=1}^H (n_h + a_h)\}}{\prod_{h=1}^H \Gamma(n_h + a_h)} \prod_{h=1}^H u_h^{n_h + a_h - 1} d\mathbf{u} \\ &= \frac{\Gamma(\sum_{h=1}^H a_h)}{\prod_{h=1}^H \Gamma(a_h)} \frac{\prod_{h=1}^H \Gamma(n_h + a_h)}{\Gamma\{\sum_{h=1}^H (n_h + a_h)\}} = \text{B}(\mathbf{a} + \bar{\mathbf{n}})/\text{B}(\mathbf{a}). \end{aligned}$$

The last integral is 1 as it represents the integral of the density of a Dirichlet random variable with parameters $n_h + a_h, h = 1, \dots, H$ over all its support. The proof for $\int (\prod_{h=1}^H u_{hy}^{n_{hy}}) d\Pi_{\mathbf{u}_y} = \text{B}(\mathbf{a} + \bar{\mathbf{n}}_y)/\text{B}(\mathbf{a})$ proceeds in the same manner. \square

Proof. of Lemma 3.2 Recalling Lemma 2.1 and factorization (2.1) we can always represent the L_1 distance $\sum_{y=1}^K \sum_{\mathbf{a} \in \mathbb{A}_V} |p_{\mathcal{Y}, \mathcal{L}(\mathcal{A})}(y, \mathbf{a}) - p_{\mathcal{Y}, \mathcal{L}(\mathcal{A})}^0(y, \mathbf{a})|$ between $p_{\mathcal{Y}, \mathcal{L}(\mathcal{A})}$ and $p_{\mathcal{Y}, \mathcal{L}(\mathcal{A})}^0$ as

$$\sum_{y=1}^K \sum_{\mathbf{a} \in \mathbb{A}_V} |p_{\mathcal{Y}}(y) \sum_{h=1}^H \nu_{hy} \prod_{l=1}^{V(V-1)/2} \{\pi_l^{(h)}\}^{a_l} \{1 - \pi_l^{(h)}\}^{1-a_l}$$

$$-p_{\mathcal{Y}}^0(y) \sum_{h=1}^H \nu_{hy}^0 \prod_{l=1}^{V(V-1)/2} \{\pi_l^{0(h)}\}^{a_l} \{1 - \pi_l^{0(h)}\}^{1-a_l},$$

with $\nu_{hy}^0 = \nu_{hy}^{*0}$ if $\boldsymbol{\pi}^{0(h)} = \boldsymbol{\pi}^{0(hy)}$ and $\nu_{hy}^0 = 0$ otherwise. Hence $\Pi\{B_\epsilon(\mathbf{p}_{\mathcal{Y}, \mathcal{L}(\mathcal{A})}^0)\}$ is equal to

$$\int 1\left(\sum_{y=1}^K \sum_{\mathbf{a} \in \mathbb{A}_V} |p_{\mathcal{Y}, \mathcal{L}(\mathcal{A})}(y, \mathbf{a}) - p_{\mathcal{Y}, \mathcal{L}(\mathcal{A})}^0(y, \mathbf{a})| < \epsilon\right) d\Pi_{\mathcal{Y}}(\mathbf{p}_{\mathcal{Y}}) d\Pi_{\nu}(\nu_1, \dots, \nu_y) d\Pi_{\pi}(\boldsymbol{\pi}^{(1)}, \dots, \boldsymbol{\pi}^{(H)}).$$

Recalling results in [Dunson and Xing \(2009\)](#) a sufficient condition for the previous integral to be strictly positive is that $\Pi_{\mathcal{Y}}\{\mathbf{p}_{\mathcal{Y}} : \sum_{y=1}^K |p_{\mathcal{Y}}(y) - p_{\mathcal{Y}}^0(y)| < \epsilon_y\} > 0$, $\Pi_{\pi}\{\boldsymbol{\pi}^{(h)}, h = 1, \dots, H : \sum_{h=1}^H \sum_{l=1}^{V(V-1)/2} |\pi_l^{(h)} - \pi_l^{0(h)}| < \epsilon_{\pi}\} > 0$ and $\Pi_{\nu}\{\boldsymbol{\nu}_y, y \in \mathbb{Y} : \sum_{y=1}^K \sum_{h=1}^H |\nu_{hy} - \nu_{hy}^0| < \epsilon_{\nu}\} > 0$ for every $\epsilon_{\pi} > 0$, $\epsilon_y > 0$ and $\epsilon_{\nu} > 0$. The large support for $\mathbf{p}_{\mathcal{Y}}$ is directly guaranteed from the Dirichlet prior. Similarly, according to Lemmas 3.1 and 3.2 in [Durante et al. \(2015\)](#) the same hold for the joint prior over the sequence of class-specific edge probability vectors $\boldsymbol{\pi}^{(h)}, h = 1, \dots, H$ induced by priors Π_Z, Π_X and Π_{λ} in factorization (2.3). Finally marginalizing out the testing indicator T and recalling our prior specification for the mixing probabilities in (3.1) a lower bound for $\Pi_{\nu}\{\boldsymbol{\nu}_y, y \in \mathbb{Y} : \sum_{y=1}^K \sum_{h=1}^H |\nu_{hy} - \nu_{hy}^0| < \epsilon_{\nu}\}$ is

$$\Pr(H_0) \Pi_{\mathbf{u}}\{\mathbf{u} : \sum_{y=1}^K \sum_{h=1}^H |u_h - \nu_{hy}^0| < \epsilon_{\nu}\} + \Pr(H_1) \prod_{y=1}^K \Pi_{\mathbf{u}_y}\{\mathbf{u}_y : \sum_{h=1}^H |u_{hy} - \nu_{hy}^0| < \epsilon_{\nu}/K\}.$$

If the true model is generated under no association, previous equation reduces to

$$\Pr(H_0) \Pi_{\mathbf{u}}\{\mathbf{u} : \sum_{h=1}^H |u_h - \nu_h^0| < \epsilon_{\nu}/K\} + \Pr(H_1) \prod_{y=1}^K \Pi_{\mathbf{u}_y}\{\mathbf{u}_y : \sum_{h=1}^H |u_{hy} - \nu_h^0| < \epsilon_{\nu}/K\},$$

with the Dirichlet priors for \mathbf{u} and $\mathbf{u}_y, y = 1, \dots, K$ ensuring the positivity of both terms. When instead $\nu_{hy}^0 \neq \nu_{hy'}^0$ for some $y, y' \in \mathbb{Y}$, the positivity of $\Pr(H_0) \Pi_{\mathbf{u}}\{\mathbf{u} : \sum_{y=1}^K \sum_{h=1}^H |u_h - \nu_{hy}^0| < \epsilon_{\nu}\}$ is no longer guaranteed, but $\Pr(H_1) \prod_{y=1}^K \Pi_{\mathbf{u}_y}\{\mathbf{u}_y : \sum_{h=1}^H |u_{hy} - \nu_{hy}^0| < \epsilon_{\nu}/K\}$ remains positive for every ϵ_{ν} under the independent Dirichlet priors for the quantities $\mathbf{u}_y, y = 1, \dots, K$, proving the Lemma. \square

References

- Agresti, A. (2002). *Categorical data analysis*. Second edition. New York: Wiley. [11](#)
- Arden, R., Chavez, R. S., Grazioplene, R., and Jung, R. E. (2010). “Neuroimaging creativity: A psychometric view.” *Behavioural Brain Research*, 214(2): 143 – 156. [3](#), [20](#)
- Benjamini, Y. and Hochberg, Y. (1995). “Controlling the False Discovery Rate: A Practical and Powerful Approach to Multiple Testing.” *Journal of the Royal Statistical Society. Series B (Methodological)*, 57(1): 289–300. [3](#), [14](#)

- Berger, J. O. and Sellke, T. (1987). “Testing a Point Null Hypothesis: The Irreconcilability of P Values and Evidence.” *Journal of the American Statistical Association*, 82(397): 112–122. [10](#)
- Bressler, S. L. and Menon, V. (2010). “Large-scale brain networks in cognition: emerging methods and principles.” *Trends in Cognitive Sciences*, 14(6): 277–290. [1](#)
- Bullmore, E. and Sporns, O. (2009). “Complex brain networks: graph theoretical analysis of structural and functional systems.” *Nature Reviews Neuroscience*, 10(3): 186–198. [2](#)
- Carlsson, I., Wendt, P. E., and Risberg, J. (2000). “On the neurobiology of creativity. Differences in frontal activity between high and low creative subjects.” *Neuropsychologia*, 38(6): 873–885. [20](#)
- Craddock, R. C., Jbabdi, S., Yan, C.-G., Vogelstein, J. T., Castellanos, F. X., Martino, A. D., Kelly, C., Heberlein, K., Colcombe, S., and Milham, M. P. (2013). “Imaging human connectomes at the macroscale.” *Nature Methods*, 10(6): 524–539. [1](#)
- Daianu, M., Jahanshad, N., Nir, T. M., Toga, A. W., Jack, C. R., Weiner, M. W., and Thompson, P. M. (2013). “Breakdown of Brain Connectivity Between Normal Aging and Alzheimer’s Disease: A Structural k -Core Network Analysis.” *Brain Connectivity*, 3(4): 407–422. [3](#)
- Desikan, R. S., Ségonne, F., Fischl, B., Quinn, B. T., Dickerson, B. C., Blacker, D., Buckner, R. L., Dale, A. M., Maguire, R. P., Hyman, B. T., Albert, M. S., and Killiany, R. J. (2006). “An automated labeling system for subdividing the human cerebral cortex on MRI scans into gyral based regions of interest.” *NeuroImage*, 31(3): 968–980. [2](#), [3](#)
- Dunson, D. B. and Xing, C. (2009). “Nonparametric Bayes Modeling of Multivariate Categorical Data.” *Journal of the American Statistical Association*, 104(487): 1042–1051. [4](#), [8](#), [22](#)
- Durante, D. and Dunson, D. B. (2014a). “Bayesian dynamic financial networks with time-varying predictors.” *Statistics & Probability Letters*, 93: 19–26. [4](#)
- (2014b). “Nonparametric Bayes dynamic modelling of relational data.” *Biometrika*, 101(4): 883–898. [3](#)
- Durante, D., Dunson, D. B., and Vogelstein, J. T. (2015). “Nonparametric Bayes Modeling of Populations of Networks.” *ArXiv e-prints*. [4](#), [5](#), [9](#), [11](#), [12](#), [20](#), [22](#)
- Erdős, P. and Rényi, A. (1959). “On random graphs.” *Publicationes Mathematicae Debrecen*, (5): 290–297. [3](#)
- Fornito, A., Zalesky, A., and Breakspear, M. (2013). “Graph analysis of the human connectome: Promise, progress, and pitfalls.” *NeuroImage*, 80: 426–444. [3](#)
- Frank, O. and Strauss, D. (1986). “Markov Graphs.” *Journal of the American Statistical Association*, 81(395): 832–842. [3](#)

- Fuster, J. M. (2000). “The Module: crisis of a paradigm.” *Neuron*, 26(1): 51–53. 1
- Genovese, C. R., Lazar, N. A., and Nichols, T. (2002). “Thresholding of Statistical Maps in Functional Neuroimaging Using the False Discovery Rate.” *NeuroImage*, 15(4): 870–878. 3
- Heilman, K. M., Nadeau, S. E., and Beversdorf, D. O. (2003). “Creative Innovation: Possible Brain Mechanisms.” *Neurocase*, 9(5): 369–379. 19
- Hoff, P. D., Raftery, A. E., and Handcock, M. S. (2002). “Latent Space Approaches to Social Network Analysis.” *Journal of the American Statistical Association*, 97(460): 1090–1098. 3, 4
- Holland, P. W. and Leinhardt, S. (1981). “An Exponential Family of Probability Distributions for Directed Graphs.” *Journal of the American Statistical Association*, 76(373): 33–50. 3
- Ishwaran, H. and Zarepour, M. (2002). “Dirichlet Prior Sieves in Finite Normal Mixtures.” *Statistica Sinica*, 12: 941–963. 12
- Jung, R. E., Segall, J. M., Bockholt, H. J., Flores, R. A., Smith, S. M., Chavez, R. S., and Haier, R. J. (2010). “Neuroanatomy of creativity.” *Human Brain Mapping*, 31(3): 398–409. 2, 20
- Kang, X., Herron, T. J., Cate, A. D., Yund, E. W., and Woods, D. L. (2012). “Hemispherically-Unified Surface Maps of Human Cerebral Cortex: Reliability and Hemispheric Asymmetries.” *PLoS ONE*, 7(9): e45582. 19
- Kantarci, B. and Labatut, V. (2013). “Classification of Complex Networks Based on Topological Properties.” In *2013 International Conference on Cloud and Green Computing*. IEEE. 11
- Krzanowski, W. (1988). *Principles of multivariate analysis: a user’s perspective*. Oxford University Press. 3, 11
- Nowicki, K. and Snijders, T. A. B. (2001). “Estimation and Prediction for Stochastic Blockstructures.” *Journal of the American Statistical Association*, 96(455): 1077–1087. 3
- Olde Dubbelink, K. T. E., Hillebrand, A., Stoffers, D., Deijen, J. B., Twisk, J. W. R., Stam, C. J., and Berendse, H. W. (2014). “Disrupted brain network topology in Parkinson’s disease: a longitudinal magnetoencephalography study.” *Brain*, 137(1): 197–207. 3
- Polson, N. G., Scott, J. G., and Windle, J. (2013). “Bayesian Inference for Logistic Models Using Pólya–Gamma Latent Variables.” *Journal of the American Statistical Association*, 108(504): 1339–1349. 11
- Robins, G. and Pattison, P. (2001). “Random graph models for temporal processes in social networks*.” *The Journal of Mathematical Sociology*, 25(1): 5–41. 3
- Roncal, W. G., Koterba, Z. H., Mhembe, D., Kleissas, D. M., Vogelstein, J. T., Burns,

- R., Bowles, A. R., Donavos, D. K., Ryman, S., Jung, R. E., Wu, L., Calhoun, V., and Vogelstein, R. J. (2013). “MIGRAINE: MRI Graph Reliability Analysis and Inference for Connectomics.” In *IEEE Global Conference on Signal and Information Processing*. IEEE. 2, 12, 19
- Rousseau, J. and Mengersen, K. (2011). “Asymptotic behaviour of the posterior distribution in overfitted mixture models.” *Journal of the Royal Statistical Society: Series B (Statistical Methodology)*, 73(5): 689–710. 9
- Rubinov, M. and Sporns, O. (2010). “Complex network measures of brain connectivity: Uses and interpretations.” *NeuroImage*, 52(3): 1059–1069. 3
- Sawyer, K. R. (2012). *Explaining Creativity: The Science of Human Innovation*. Oxford University Press. 20
- Sellke, T., Bayarri, M. J., and Berger, J. O. (2001). “Calibration of p Values for Testing Precise Null Hypotheses.” *The American Statistician*, 55(1): 62–71. 14
- Shobe, E. R., Ross, N. M., and Fleck, J. I. (2009). “Influence of handedness and bilateral eye movements on creativity.” *Brain and Cognition*, 71(3): 204–214. 20
- Simpson, S. L., Moussa, M. N., and Laurienti, P. J. (2012). “An exponential random graph modeling approach to creating group-based representative whole-brain connectivity networks.” *NeuroImage*, 60(2): 1117–1126. 3
- Snijders, T. A. B., Pattison, P. E., Robins, G. L., and Handcock, M. S. (2006). “New Specification for Exponential Random Graph Models.” *Sociological Methodology*, 36(1): 99–153. 4
- Stam, C. J. (2014). “Modern network science of neurological disorders.” *Nature Reviews Neuroscience*, 15(10): 683–695. 2
- Stephens, M. (2000). “Dealing with label switching in mixture models.” *Journal of the Royal Statistical Society: Series B (Statistical Methodology)*, 62(4): 795–809. 12
- Stirling, J. and Elliott, R. (2008). *Introducing Neuropsychology*. Routledge. 1
- Takeuchi, H., Taki, Y., Sassa, Y., Hashizume, H., Sekiguchi, A., Fukushima, A., and Kawashima, R. (2010). “White matter structures associated with creativity: Evidence from diffusion tensor imaging.” *NeuroImage*, 51(1): 11–18. 20
- Tang, L., Wang, X., and Liu, H. (2011). “Community detection via heterogeneous interaction analysis.” *Data Mining and Knowledge Discovery*, 25(1): 1–33. 3
- Wang, J., He, L., Zheng, H., and Lu, Z.-L. (2014). “Optimizing the Magnetization-Prepared Rapid Gradient-Echo (MP-RAGE) Sequence.” *PLoS ONE*, 9(5): 1–12. 1
- Xing, E. P., Fu, W., and Song, L. (2010). “A state-space mixed membership blockmodel for dynamic network tomography.” *The Annals of Applied Statistics*, 4(2): 535–566. 3
- Zalesky, A., Fornito, A., and Bullmore, E. T. (2010). “Network-based statistic: Identifying differences in brain networks.” *NeuroImage*, 53(4): 1197–1207. 3

Acknowledgments

This work was partially funded by the Office of Naval Research Grant: N00014-14-1-0245. The authors would like to thank Rex E. Jung and Sephira G. Ryman for the brain connectivity data and creativity scores funded by the John Templeton Foundation (Grant 22156) entitled “The Neuroscience of Scientific Creativity.” The authors are also grateful to William G. Roncal and Joshua T. Vogelstein for help in accessing the connectome data.